Journal of Applied Fluid Mechanics , Vol. 9, No. 5, pp. 2333-2345, 2016.
Available online at www.jafmonline.net, ISSN 1735-3572, EISSN 1735-3645.

Numerical Modeling of 2-D and 3-D Flows using Artificial Compressibility Method and Collocated Mesh

Y. Aghaee-Shalmani[1†] and H. Hakimzadeh[2]

[1] *Department of Civil and Mechanical Engineering, Khomeinishahr Branch, Islamic Azad University, Khomeinishahr, Isfahan, Iran*
[2] *Dept. of Civil Engineering, Sahand Univ. of Technology, Tabriz, Iran*

† *Corresponding Author Email*: *y.aghaee@iaukhsh.ac.ir*

(Received October 20, 2013, ; accepted November 4, 2015,)

ABSTRACT

In this paper, applications of a numerical model on simulation of two and three-dimensional flows are presented. This model solves Navier-Stokes equations using finite volume method and large eddy simulation (LES) in a collocated mesh. Artificial compressibility method with dual time stepping is used to solve the time dependent equations. Also a modified momentum interpolation method (MIM) based on the unsteady flows is deployed to overcome the non-physical pressure oscillation. Capability of the presented numerical code for flow simulation, is assessed by application for two-dimensional square and three-dimensional lid-driven cavity flows. Numerical results of cavity flow presents very good agreement with the numerical and experimental data of other existent researches.

Keywords: Artificial compressibility; Collocated mesh; MIM; LES; Lid-driven cavity.

NOMENCLATURE

C_s	Smagorinsky parameter
L	length of cavity
l_s	sub-grid length scale
m	iterative numbers of the physical time
N	total number of computational cells
n	iterative numbers of the pseudo-time
P	pressure
r	iteration level of Gauss-Seidel method
Re	Reynolds number
S	cell surface area
S_{ij}	strain rate tensor
U_{in}	Lid-driven velocity
U_{rms}	root mean square of $\bar{u}$ velocity
$\bar{u}_i$	filtered velocities
$\hat{u}_i$	time-averaged velocities
$\acute{u}_i$	instantaneous velocities
W_{rms}	root mean square of $\bar{w}$ velocity
x_i	cartesian coordinate
β	artificial compressibility parameter
Δ	volume of a computational cell
Δt	physical time step
$\Delta\tau$	artificial time step
δ_{ij}	Kronecker delta
κ	Von Karman constant
ν	kinematic viscosity of fluid
ν_t	sub-grid eddy-viscosity coefficient
ρ	density f fluid
τ_{ij}	sub-grid turbulence stress

1. INTRODUCTION

Navier-Stokes (NS) equations are the most used equations to investigate the hydrodynamic phenomena at different problems. Solution of these equations is achievable with the numerous methods that were proposed by researchers to provide the coupling between pressure and velocity field. The most well known method is the pressure correction method which was first proposed by Harlow and Welch (1965). The other methods are fractional step and artificial compressibility (AC) method. It seems that there is no specific superiority among these methods. However, some researchers mentioned the superiority of AC method in accelerating convergence in comparison to the other numerical methods (Tamamidis *et al.* 1996). The concept of artificial compressibility, **was** originally proposed by Chorin (1967) for solv-

ing steady flows. AC method is **developed** for unsteady solution with two different methods. The first method is the application of the large artificial compressibility parameter (β) which called single time stepping and the second one is dual time stepping. Louda *et al.* (2008) studied both single and dual time stepping methods to model unsteady flows. Aghaee and Hakimzadeh (2010), used the single time stepping method to simulate the unsteady flow around a vertically placed circular cylinder and acceptable results were obtained. With increasing the power of computers and processors, the accuracy of the numerical models can be improved. Numerous researches used dual time stepping method as an accurate method to solve NS equations numerically (Breuer 1993; Kim and Menon 1999; Fu *et al.* 2009).

Dual time stepping method can be used along with staggered or collocated grids. The simplicity of the collocated grids is retained by storing all the unknowns (Cartesian velocity components and the pressure) at the cell center. Note that if a collocated (non-staggered) grid is used and the velocity derivatives in the continuity equation and the pressure derivatives in the momentum equation are central-differenced, velocity and pressure are decoupled (Kim and Menon 1999). This decoupling eventuate non-physical pressure oscillation in computational domain. It has been noted by researchers that the AC method can slightly remove the pressure oscillation. However, to overcome the pressure oscillation, different approaches have been proposed by the researchers namely, one-sided discretization, flux-splitting (Steger and Warming 1981; Harten 1983; Harten 1987; Gosse 2000), elliptic-corrected linear interpolation; (Armfield 1991), regularized central difference; (Strikwerda 1984; Kim and Menon 1999), consistent flux reconstruction (CFR) (Roy and Bandyopadhyay 2006) and momentum interpolation method (MIM) proposed by Rhie and Chow (1983). In addition to the aforementioned methods, the artificial viscosity has been widely used in the literature to overcome the pressure oscillation because of using collocated mesh (Paik *et al.* 2007; Prokop and Kozel 2010). Nowadays, application of different methods of MIM is increasing because of good performance and easy programming in comparison with other non-oscillatory methods and staggered meshes.

In this study we aim to apply artificial compressibility method with dual time stepping and MIM method for numerical simulation of flow in 2-D and 3-D domains. A code based on the finite volume method and turbulent model of large eddy simulation are used to solve the governing equations. The focus of the paper is to develop a suitable model that is based on artificial compressibility with dual time stepping method on the collocated grids. Numerical model of present study uses the modified MIM for unsteady flows and is the combination of recent methods of MIM which proposed by Cubero and Fueyo (2007) and Li and Gu (2010). Some modification to these methods, make the proposed method compatible with numerical algorithm. The applications of the developed numerical model to the two-dimensional (2-D) and three-dimensional (3-D) cavity flows are presented in this study. The 2-D results is compared with the existent numerical results of the 2-D cavity flows with staggered or collocated meshes. The 3-D code is applied in lid driven cavity flow to show the capability of the artificial compressibility method with collocated mesh and MIM technique for modeling the real flows. The results are validated against existent experimental data.

2. NUMERICAL MODEL

2.1 Governing Equations and the Sub-Grid Model

Present numerical model, use Large eddy simulation (LES) to deal with the turbulence. In LES, the large scales of the turbulence which are larger than the filter size (grid size) are directly solved in the computational domain (Breuer 1998; cheng *et al.* 2003). To achieve this target, the Navier-Stokes and continuity equations are spatially filtered as follows

$$\frac{\partial \bar{u}_i}{\partial x_i} = 0, , \qquad (i = 1,2,3)$$
$$\frac{\partial \bar{u}_i}{\partial t} + \frac{\partial \bar{u}_i \bar{u}_j}{\partial x_j} = -\frac{1}{\rho}\frac{\partial \bar{p}}{\partial x_i} + \nu \frac{\partial^2 \bar{u}_i}{\partial x_j \partial x_j} - \frac{\partial \tau_{ij}}{\partial x_j} \quad (1)$$

where x_i are the Cartesian coordinates, ρ is the fluid density, p is the pressure and ν is the kinematic viscosity of the fluid. τ_{ij} is the sub-grid turbulence stress and the over bar shows the spatial filtering. The eddy viscosity concept for the sub-grid stress is

$$\tau_{ij} - \frac{1}{3}\delta_{ij}\tau_{kk} = -2\nu_t \bar{S}_{ij}, \quad (2)$$

where ν_t is the **sub-grid scale** (**SGS**) eddy-viscosity coefficient. δ_{ij} is the Kronecker delta. $\bar{S}_{ij}$ is the strain rate tensor for the resolved scales. defined by

$$\bar{S}_{ij} = \frac{1}{2}\left(\frac{\partial \bar{u}_i}{\partial x_j} + \frac{\partial \bar{u}_j}{\partial x_i}\right). \quad (3)$$

The SGS eddy-viscosity may be written as a function of the strain rate and sub-grid length scale , l_s, as follows

$$\nu_t = l_s^2 |\bar{S}_{ij}|, \tag{4}$$

where $|\bar{S}_{ij}| = \sqrt{2\bar{S}_{ij}\bar{S}_{ij}}$ and $l_s = min(\kappa y, C_s \triangle^{1/3})$. $\triangle$ is the volume of the computational cell, κ is the Von Karman constant ($\kappa = 0.42$) and y is the distance to the nearest wall. C_s is the Smagorinsky SGS parameter. The value of Cs depends on the problem. However the large values of Cs cause excessive damping of the large-scale fluctuations and very low values (Cs < 0.1) may cause convergence problem (Lam and Lin 2008). The optimum values of the Cs can be found in the literature as 0.1 < Cs < 0.14. In this research the parameter Cs is adopted as 0.11.

2.2 Dual-Time Stepping and Discretization

The AC method is introduced by adding the time variant term of pressure in continuity equation which this term also includes the artificial compressibility parameter (β). By adding the temporal term to the continuity equation, the method becomes suitable for steady flow simulation. For unsteady solution the solver requires the addition of a pseudo (artificial) time derivative term to the momentum equations as follows (Kim and Menon 1999).

$$\frac{1}{\rho\beta^2}\frac{\partial \bar{p}}{\partial \tau} + \frac{\partial \bar{u}_i}{\partial x_i} = 0, \qquad (i = 1,2,3)$$
$$\frac{\partial \bar{u}_i}{\partial \tau} + \frac{\partial \bar{u}_i}{\partial t} + \frac{\partial \bar{u}_i \bar{u}_j}{\partial x_j} = -\frac{1}{\rho}\frac{\partial \bar{p}}{\partial x_i} + \nu \frac{\partial^2 \bar{u}_i}{\partial x_j \partial x_j} - \frac{\partial \tau_{ij}}{\partial x_j} \tag{5}$$

where t is the physical time and τ is the artificial (pseudo) time. In dual time stepping method, instead of solving each time-step in the physical time, the problem is transformed into a sequence of steady-state computations in the artificial times. Numerical experiments show that the number of iterations depends on the problem. However, for large physical time step and large values of the AC parameter (β), the number of iterations is increased. The optimum value of β has been proposed by researchers as $\beta^2 = \alpha {u_i}^2$, where α varies from 1 to 6. Marx (1994) and Kim and Menon (1999) used $\alpha = 3$ and $\alpha > 6$ for their numerical models, respectively. The value of β in the present study is adopted as fix and slightly larger than the value of inlet velocity. Euler Second order backward difference method is used for discretization of the physical time. This scheme is very stable and dissipative and insensitive to the stiffness of the problem (Kim and Menon 1999). Since time accuracy in pseudo time is of no concern, the time derivatives in discretized equations should be discretized using methods chosen to maximize efficiency and robustness (Muldoon and Acharya 2007). Breuer (1993) mentioned that for artificial time, the backward first order Euler method is sufficient. Therefore, an implicit formulation can be written as follows for the momentum equation in x direction,

$$\frac{u^{m+1} - u^m}{\Delta\tau} + \frac{3u^{m+1,n+1} - 4u^n + u^{n-1}}{2\Delta t} = Rez(u) \tag{6}$$

where the superscripts m and n denote the iterative numbers of the pseudo and physical times, respectively. $Rez(u)$ include the convective and diffusive terms. Convective terms are discretized using the QUICK scheme. The differed correction method of Khosla and Rubin (1974) is used to deal with convective terms as follows:

$$(\mathbf{F_c})^{m+1}_{QUICK} = (\mathbf{F_c})^{m+1}_{Central} + \left[\left(\mathbf{F_c}\right)^{m}_{QUICK} - (\mathbf{F_c})^{m}_{Central}\right] \tag{7}$$

The implicit part of the convective terms is linearized by Newton method (Sheu and Lin 2004). Viscous terms are discretized using the second-order central scheme and the pressure gradient is approximated by central scheme. In the discretized equation, seven cells are retained as implicit and the other cells transferred to the right hand side of discretized equation as explicit. The implicit point Gauss-Seidel method with under relaxation is then used to solve linearized system with seven-diagonals matrix. The values of the physical tim step (Δt) and artificial time step ($\Delta\tau$) depend on the discretization scheme. Due to using implicit time discretization in this study, there is no constraint for choosing the value of artificial time step and then, convergence is achieved by relatively large artificial time steps and few pseudo iteration.

2.3 Collocated Mesh

As aforementioned, the momentum interpolation method is attractive because of its efficiency and easy programming. The original momentum interpolation was reported by Rhie and Chow (1983); however, this method was dependent to the relaxation parameter and time step. Majumdar (1988), Miller and Schmidt (1988) and Choi (1999) in separate researches presented schemes which were independent of the relaxation factor. Later, Yu *et al.* (2002)

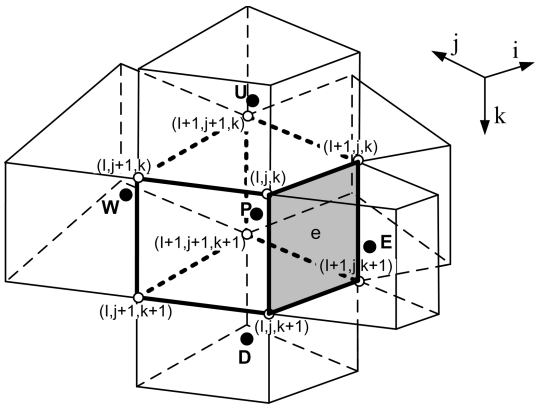

Fig. 1. Schematic view of computational cell and notations. All of the variables are saved at center of the cells.

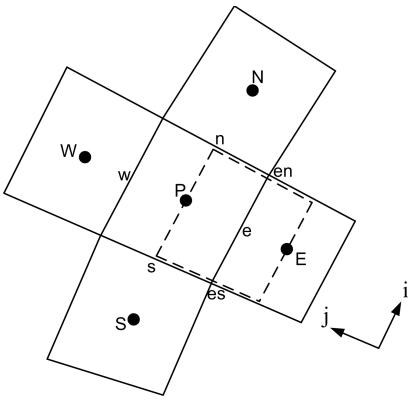

Fig. 2. 2-D view of the collocated computational control volume and the auxiliary cell (dashed line) to compute the interface velocity.

applied the MIM that was independent of the time step. Cubero and Fueyo (2007) presented a compact method that included the original MIM and was time step and relaxation free method. This method has been proposed for different time discretizations. Also, a similar MIM for time marching solutions has been presented by Li and Gu (2010). They showed that the proposed MIM is stable and independent of the step size of physical times for all-speed flows.

For the present work, combination of the the methods proposed by Cubero and Fueyo (2007) and Li and Gu (2010) is applied to overcome the pressure oscillation due to collocated grid. Fig. 1 shows a cell centered collocated structured mesh with surrounded nodes used in discretized equations in this article. For an specific surface e (shown in Fig. 1) the momentum interpolation method can be applied. The interface velocity components at e interface is expressed by:

$$u_e^{n+1} = \lfloor u \rfloor_e^{m+1} + \frac{1}{\rho}\left\{ \left\lfloor \frac{\frac{\partial \bar{p}}{\partial x}}{a_p} \right\rfloor_e - \left(\frac{\frac{\partial \bar{p}}{\partial x}}{a_p} \right)_e \right\}^m - \frac{2}{\triangle t}\left\{ \left\lfloor \frac{u}{a_p} \right\rfloor_e - \left(\frac{u}{a_p} \right)_e \right\}^n - \frac{-0.5}{\triangle t}\left\{ \left\lfloor \frac{u}{a_p} \right\rfloor_e - \left(\frac{u}{a_p} \right)_e \right\}^{n-1}, \quad (8)$$

The first term at the right hand side of the Eq. (8), presents the averaged velocities of two adjacent cells P and E. The next terms in accolade, show the original momentum interpolation terms proposed by (Rhie and Chow 1983). This terms mainly control the pressure oscillation and add dissipation to the numerical code.

The next two terms show the modified original momentum interpolation due to existence of the physical time steps in unsteady solution. In this research, the terms include the relaxation parameter does not exist because of the algorithm of the numerical code. In each artificial-time iteration, first, the momentum equations are solved by Gauss-Seidel method and the new values of the velocities by using relaxation are renewed until the convergence is achieved, then, the momentum interpolation is applied to calculate the interface velocities. Since, we did not use the MIM in each Gauss-Seidel iteration, we did not apply relaxation terms in the presented modified MIM. The interpolated and calculated interface pressure gradients in Eq. (8) can be calculated as follows

$$\left\lfloor \frac{\frac{\partial \bar{p}}{\partial x}}{a_p} \right\rfloor_e = (1-\lambda_e)\left(\frac{\frac{\partial \bar{p}}{\partial x}}{a_p} \right)_P + \lambda_e \left(\frac{\frac{\partial \bar{p}}{\partial x}}{a_p} \right)_E,$$
$$\left(\frac{\frac{\partial \bar{p}}{\partial x}}{a_p} \right)_e = \left(\frac{\partial \bar{p}}{\partial x} \right)_e \left((1-\lambda_e)\frac{1}{a_{p\,P}} + \lambda_e \frac{1}{a_{p\,E}} \right). \quad (9)$$

Note that the other variables in the "$\lfloor\rfloor$" and "()" in Eq. 8 can be written in a similar way. a_p is the algebraic coefficient which depends on the discretized scheme. The sub-scripts e, P and E used in Eq. 9 are the interface and central points of the control volumes (see Fig. 2). For non-uniform grids, λ_e is a fraction of the distance between nodes P and E, which has been defined as $\lambda_e = \frac{\delta l_{Pe}}{\delta l_{PE}}$ in this research. Where δl_{Pe} is the distance between nodes P and e and δl_{PE} is the distance between nodes P and E.

The resulted interface velocities from MIM are only applied to the continuity equation to calculate the new value of the pressure.

2.4 Boundary Condition and Numerical Algorithm

For the governing equations, the following boundary conditions are used for the current study.

At the inlet boundary (top lid of the cavity), uniform velocities are imposed ($u = U_{in}, v = w = 0$), where U_{in} is the inlet velocity (top lid velocity of the cavity). For the solid walls, no-slip condition are used. For the pressure in all boundaries, the Neumann condition is also imposed. The ghost cells are created to apply the boundary condition at all of the boundaries. For the velocities and pressures at the boundaries, the second order discretization are used. In the present study, the non-blocking Message Passing Interface (MPI) send and receive functions are used to transfer data between processors. Because of using the QUICK scheme for convective terms and also the momentum interpolation method, it is needed to pass the data of two layers of the decomposed domains between two adjacent domains (processors). The convergence in each artificial time is checked by the following L_2 norm (Nithiarasu 2003)

$$Res_p = \frac{1}{N}\sum_{i=1}^{N}\left[\frac{1}{\rho\beta^2}\left(\frac{p^{m+1}-p^m}{\Delta\tau}\right)\right]^2, \quad (10)$$

where N is the total number of numerical cells. For convergence, the above L_2 norm is set to a constant value 1×10^{-6}. For Gauss-Seidel iteration, the sum of the velocity residuals are calculated in each iteration as follows

$$Res_{\mathrm{vel}} = \frac{\sum_{i=1}^{N}[\sum_{j=1}^{3}|u_j{}^{r+1}-u_j{}^{r}|]}{\sum_{i=1}^{N}[\sum_{j=1}^{3}|u_j{}^{r+1}|]}, \quad (11)$$

where $u_j, j = 1,2,3$ are the u, v and w velocities, respectively and r is the iteration level of Gauss-Seidel. This residual at the end of Gauss-Seidel iteration should be lower than 1×10^{-6}. The overall algorithm of the numerical solution is as follows:

1) Solve the momentum equations using the Gauss-Seidel method.
2) If $Res_{\mathrm{vel}} < 10^{-6}$, then exit Gauss-Seidel iteration.
3) Apply the boundary conditions.
4) Calculate the interface velocities by MIM.
5) Insert the interface velocities in continuity equation and compute the new value of pressure by *AC* method.
6) Check the residual of pressure.
7) If $Res_p > 10^{-6}$, then go to the next iteration for artificial time step and start from the stage number 1.
8) If $Res_p < 10^{-6}$, then update the values of the pressure and velocities and go to the next iteration for physical time step and start from the stage number 1. For parallel modeling the residuals are calculated in each decomposed domain (processor) and the maximum of them is used to check the criteria of solution.

3. APPLICATION OF THE MODEL AND RESULTS

Application of the model presents the ability of the proposed numerical model. For this reason, the results of such studies are usually verified by the existent experimental data or compared with accurate numerical results in literature.

In this study we apply our numerical code on 2-D and 3-D cavity flows and compare the results with other numerical or experimental results. Lid driven cavities have simple geometries. Nonetheless, the flow structures in these simple domains are so complex with various turbulence scales. Due to various states exhibited by the flow at higher Re, it is a very challenging problem to study, particularly in obtaining computational results as it requires accurate methods with long averaging times. All of the 2-D models has been run on single processor of a dual-core DELL LATITUDE D830 with 2GB RAM and 2.2 GHz CPU. In each run the used RAM was about 1.2 GB. Also, the 3-D models used processors of 2.2 GHz AMD Opteron of national high performance supercomputer of Isfahan university of technology.

3.1 Literature of Cavity Flow

Numerous papers in literature of cavity modeling deal with the two-dimensional problem with different method of solution like finite difference, finite volume or finite element with various approaches (Ghia *et al.* 1982; Sahin and Owens 2003; Erturk *et al.* 2005; Hachem *et al.* 2010). The most prominent experimental data for 3-D lid-driven cavity flow is found in study of Prasad and Koseff (1989) which is very useful reference to validate the numerical results. In the mentioned reference, different Reynolds numbers up to 10,000 have been tested and various spanwise aspect ratios (SAR) applied. Also, direct numerical simulation (DNS) of cavity can be found in literature at different Reynolds num-

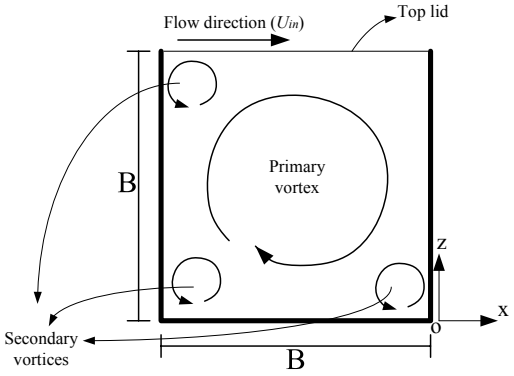

Fig. 3. Schematic view of 2-D cavity flow.

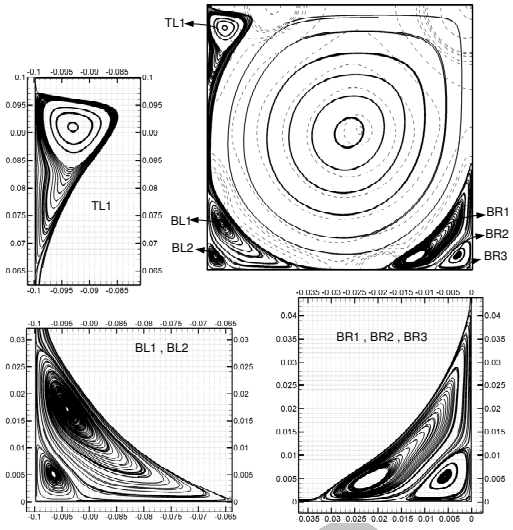

Fig. 4. Time averaged stream-lines and contours of the pressure (dashed lines) of Lid-Driven cavity $Re = 10000$ with grid 200×200. The maximum and minimum values of the pressure contours are at top-right and top-left corners of the cavity and equal to 13.06 (Pa) and -1.85 (Pa), respectively. At center of the primary vortex the value of pressure contour is -0.65 (Pa).

bers higher than 12,000 (Leriche and Gavrilakis 2000; Leriche 2006). Moreover, there are 3-D cavity flow simulation using Large Eddy Simulation (LES) in studies (Zang *et al.* 1993; Kim and Menon 1999; Huang and Li 2010). The common used spanwise aspect ratio in the literature for 3-D numerical modeling of cavity at Re=10,000, is 0.5 to reduce simulation cost. Also, some examples of cubical lid driven cavity with SAR=1 exist at high Reynolds numbers in work of Hassan and Barsamian (2001) who, used different wall models for large eddy simulation of lid-driven cavity flow and Premnath *et al.* (2009) who used lid driven-cavity flow for validating their proposed Lattice-Boltzmann method.

In this section, the validation of the presented numerical model is carried out as follows: 1) two-dimensional square lid-driven cavity flow. The Reynolds number $Re = LU_{in}/\nu$ equal to 10,000 is used based on the square length L and the velocity of the lid U_{in}. 2) three-dimensional cubical lid driven cavity flow with $Re = 10,000$. First, square lid-driven cavity is discussed and then the flow in a cubical lid-driven cavity will be presented.

3.11 2-D Lid-Driven Cavity Flow

The importance of this problem is due to existence of the complex flow structure in such a simple geometric domain. Fig. 3 indicates the schematic view of the square cavity flow. To capture all the important structures in cavity, the sufficient number of grids are needed. In this study, for square cavity, two nonuniform grids (100×100 and 200×200) are used. Clustering of the grids is applied near the walls and inlet boundary. The ratio of clustering is about 1.02. The results of the numerical model are compared to the ones of the other researches, namely: Ghia *et al.* (1982), Erturk *et al.* (2005) and experiment of Prasad and Koseff (1989).

To explain the results of the flow we need to average the LES results in physical time. Time averaging is carried out for sufficient period of the physical time (in this research about 100,000 physical time steps).

Figure 4 presents the averaged stream lines of the velocities using the grid 200×200. As can be seen in this figure, the primary vortex is located at about the center of square and has a clockwise rotation (lid moves from left to right). In addition to the primary vortex, a number of vortices appear at the down-right and down-left of the square cavity. Based on the results of the other researchers, at down-right corner of square cavity, for the Re up to 1000 only one vortex appears. However, for $Re = 1000$ up to $Re = 7500$ two vortices and for $Re = 7500$ up to $Re = 10000$ three vortices appear in this corner of the square (Ghia *et al.* 1982; Sahin and Owens 2003; Erturk *et al.* 2005). These vortices can be observed in the present model results and are named as $BR1$, $BR2$ and $BR3$ as depicted in Fig. 4. For the down-left corner of the square, the number of vortices are two ($BL1$ and $BL2$) for $Re = 10000$ and finally at top-left corner,

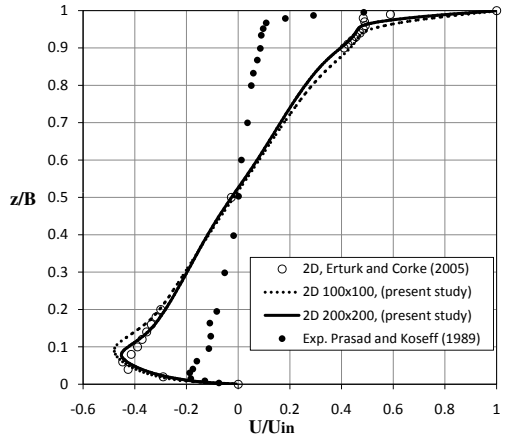

Fig. 5. Comparison of the mean normalized u-velocities at centerline of the square cavity with 2-D numerical and experimental results, $Re = 10000$.

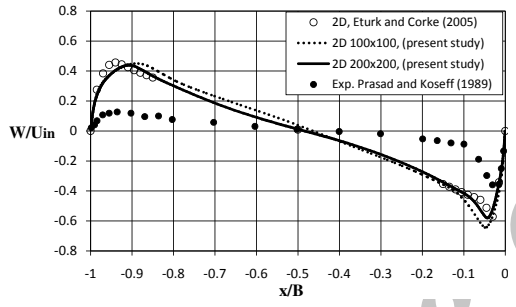

Fig. 6. Comparison of the mean v velocities at centerline of the square cavity with 2-D numerical and experimental results, $Re = 10000$.

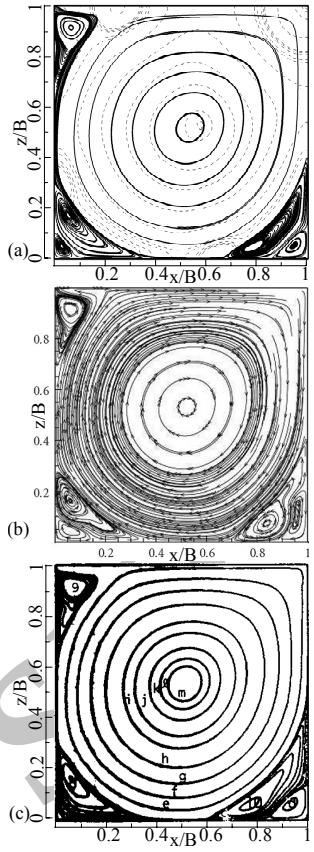

Fig. 7. Comparison of the streamlines of the square cavity flow with 2-D numerical and experimental results, $Re = 10000$. (a) numerical modeling of Ketabdari and Saghi (2011) , (b) present study, (c) numerical results of Ghia *et al.* (1987).

one vortex ($TL1$) is generated. Erturk *et al.* (2005) mentioned that grid numbers more than 513×513 can capture the third vortex ($BL3$) at down-left corner of the cavity. This vortex can not be observed for the current numerical results. However, good agreement was obtained in sense of number of vortices and stream lines in comparison with the 2-D numerical results of Erturk *et al.* (2005) and Ghia *et al.* (1982).

Table 1 compares the locations of the centers and sizes of the mentioned vortices with the numerical results of Ghia *et al.* (1982). It should be noted that, data in the table is based on the origin at the bottom-left corner, and x-axis is considered from left to right. The notations *height* and *length* in Table 1 are the normalized vertical and horizontal length of the vortices, respectively. The values were normalized by the length of the cavity. Overall agreement with numerical results of Ghia *et al.* (1982) is very good except for the $BL2$ in which over prediction for length and height of the vortex can be observed.

In Figs. 5 and 6, the time averaged velocities along vertical and horizontal lines at the center of the cavity are compared with 2-D numerical results of Erturk *et al.* (2005) and experimental results of Prasad and Koseff (1989). The results of two meshes (100×100 and 200×200) are close to each other. However, the results of grid 200×200 presents better agreement with results of Erturk *et al.* (2005) than the coarser grid. It should be noted that, the minimum grid numbers used in numerical modeling of Erturk *et al.* (2005) is 401×401.

In Fig. 7 the stream lines in cavity flow are compared. In this figure the results of the present study with modified MIM is compared

Table 1 Properties of different vortices in square cavity for $Re = 10,000$

	PV §	PV LES	TL1 §	TL1 LES	BL1 §	BL1 LES	BL2 §	BL2 LES	BR1 §	BR1 LES	BR2 §	BR2 LES
Location(x)	0.5117	0.5242	0.0703	0.0702	0.0586	0.0596	0.0156	0.03	0.7656	0.7781	0.9336	0.9424
Location(z)	0.5333	0.5179	0.9144	0.912	0.1641	0.1702	0.0195	0.05	0.0586	0.0524	0.0625	0.0545
Length	-	-	0.1589	0.1522	0.3438	0.351	0.0352	0.073	0.3906	0.329	0.1706	0.1478
Height	-	-	0.3203	0.323	0.2891	0.286	0.0441	0.11	0.4492	0.431	0.1367	0.1204

§ Ghia *et al.* (1982)

with results of Ketabdari and Saghi (2011), who modeled the 2-D cavity flow by LES and original version of MIM in their work. Also, the results of Ghia *et al.* (1982) included in this figure as a bench mark solution of cavity. As can be seen in this figure, the streamlines of the present study are in better agreement with the study of Ghia *et al.* (1982) in comparison with results of Ketabdari and Saghi (2011).

Despite the agreement with 2-D results, there is a big gap between 2-D results of present study and experimental data of Prasad and Koseff (1989). The discrepancies are due to the inherent behavior of 3-D cavity flow. Shankar and Deshpande (2000) mentioned that 2-D models for lid driven cavities are not adequate and they can seriously misleading. Also, Chen and Doolen (1998) showed the difference of the 2-D cavity model results with 3-D modeling and experimental data.

3.12 3-D Lid-Driven Cavity

In this part, application of the model to the 3-D cubical cavity flow is presented. The flow structure of the 3-D cavity flow is similar to the 2-D one but it is more complex due to the existence of side walls (Kim and Menon 1999). It seems that the flow regime at central part of the cavity is to some extent laminar, however, in the corners of the cavity the main structure of the flow is 3-D and there are a lots of three-dimensional effects and the flow is turbulent. The $Re = \frac{U_{in}B}{\nu}$ of the flow in this case is based on the experiment of Prasad and Koseff (1989).

The schematic view of the 3-D cavity is shown in Fig. 8. The spanwise aspect ratio of cavity ($SAR = L/B$) is equal to 1. The domain size in three direction equals to 0.15 m and the lid velocity is 0.0667 m/s.

This domain size and flow velocity correspond to Re number equals to 10,000. The velocity is imposed at the top surface of the cavity (U_{in}) and for other walls the no-slip boundary con-

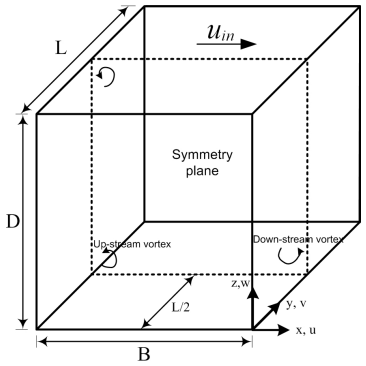

Fig. 8. Schematic view of 3-D lid driven cavity.

dition is used. Simulations are carried out by using grid 50^3 and 72^3. In order to resolve the boundary layer near the top lid and the walls, the non-uniform grids are generated where the grid stretching ratio is smaller than 1.02. The grid clustering is generated at all of the walls. The dimensionless size ($\Delta x/B$) of the smallest element edge is 1.2×10^{-3} and the largest element size of the cavity is 3.0×10^{-2} for grid 72^3. Results of the solution with coarse grid 50^3 showed significant different from grid 72^3. Also the model was tested with grid 81^3 which this finer mesh solution yielded slightly better agreement with the measurements than grid 72^3 , but in general the calculated flow fields on both grids were very similar to each other. Fig. Therefore, it seams that for cavity simulation using present numerical modeling, the grid 72^3 has adequate resolution to show the scales of flow structures. In Table 2 the magnitudes of flow velocity at symmetry plane of the cavity resulted from different grid number were compared against the experiment of Prasad and Koseff (1989) and direct numeri-cal solution of Leriche and Gavrilakis (2000).

In simulation, physical and virtual time steps are set to 8.0×10^{-3} and 1.5×10^{-3} s, respectively. In this study the physical time-step was selected as minimum as possible to en-sure that, the time-scale effect on the turbulent

Table 2 Comparison of the value of the velocities in 3-D Lid-driven cavity for $Re = 10,000$

Reference	Grid	$(u/U_{in})_{center}$	$(w/U_{in})_{center}$	$min(u/U_{in})$	$max(u/U_{in})$	$min(w/U_{in})$	$max(w/U_{in})$
Present(LES)	50^3	0.0021	0.023	-0.2310	1.00	-0.4355	0.1295
Present(LES)	72^3	0.0017	0.018	-0.2201	1.00	-0.4069	0.1227
Present(LES)	81^3	0.0016	0.016	-0.2102	1.00	-0.3951	0.1223
(DNS)†	129^3	-0.0055	0.011	-0.1674	1.00	-0.3633	0.1102
(Exp.)‡	–	0.0014	0.011	-0.1875	1.00	-0.3593	0.1265

†Leriche and Gavrilakis (2000) , ‡Prasad and Koseff (1989)

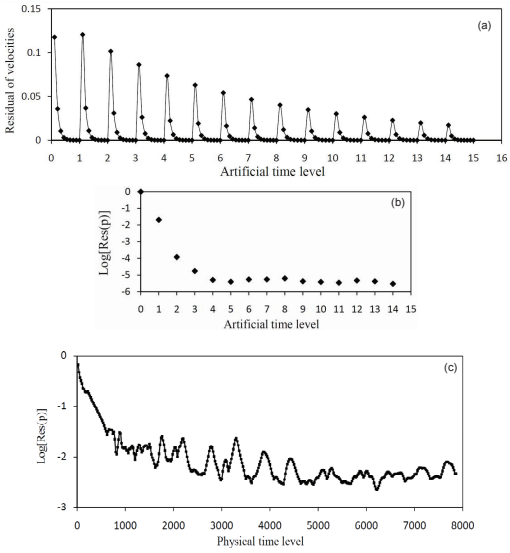

Fig. 9. Convergence history of dual time stepping, (a) Residual of velocities, (b) Residual of pressure in one physical time and (c) Residual of pressure in different physical time levels.

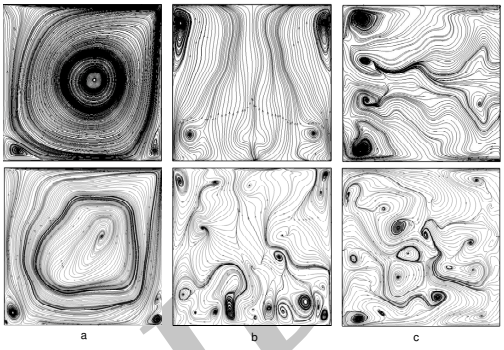

Fig. 10. Mean (top) and instantaneous (bottom) stream lines at different planes of the cavity (a) x-z plane $y/B = 0.5$ (b) y-z plane $x/B = -0.5$ and (c) x-y plane $z/B = 0.5$, $Re = 10000$.

structure be negligible. The implicit solver of this study allow to increase the ef-ficiency of the numerical code. However, we selected the value of time-step slightly larger than the explicit solver. The maximum num-ber of iteration in virtual time (pseudo time) is 30 and the minimum is 5. Time averaged val-ues of velocities and variables are obtained by averaging over more than $150B/U_{in}$ s. It should be noted that the averaging time interval of the experiment of Prasad and Koseff (1989) at each data point is given as 5.46 minutes. Fig. 9 shows the history of the convergence of 3-D numerical solution of cavity flow for dual time stepping method.

Figure 10 shows the mean and instantaneous stream lines in different 2-D planes of cubical cavity. As can be seen in this figure, for mean stream lines in mid plane of the cavity (x-z plane $y/B = 0.5$) there are three vortices. In y-z plane *i.e.,* $x/B = -0.5$ four vortices and in plane of x-y *i.e.,* $z/B = 0.5$ there are six vortices. It should be noted that the stream lines for both of the planes y-z and x-y are symmetric. Overall pattern of stream lines of the instantaneous flow are very complex as can be seen in Fig. 10.

Figures 11 and 12 present the time averaged velocities along the mid plane of the cube in which are compared to the experiment of Prasad and Koseff (1989) and direct numerical solution of Leriche and Gavrilakis (2000). The mean velocities presented in these figures have been normalized by the top lid velocity (U_{in}). The maximum velocity in x direction is at top lid of the cavity. At top-right corner of the cavity, the flow direction is changed and the downward flow is generated because of the high pressure gradient at this location. The maximum mean downward velocity is reached near the top right corner of cavity at location $z/B = 0.05$ and $x/B \approx -0.01$ from the the top lid and downstream wall, respectively. From this location to the lower lid of cavity we observe a downward jet like flow. The mean downflow velocity at mid plane of the cavity at center line of it *i.e.,* $z/B = 0.5$ is $w/U_{in} = -0.42$. This jet flow after hitting the bottom wall spreads in the spanwise direction and the generated turbulence of this impact,

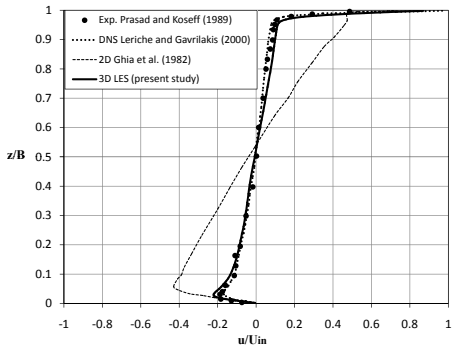

Fig. 11. Comparison of mean u velocities on the centerline ($x/B = -0.5, y/B = 0.5$) in the mid-plane of the cavity with experimental data and DNS results. Re=10000 and SAR=1.

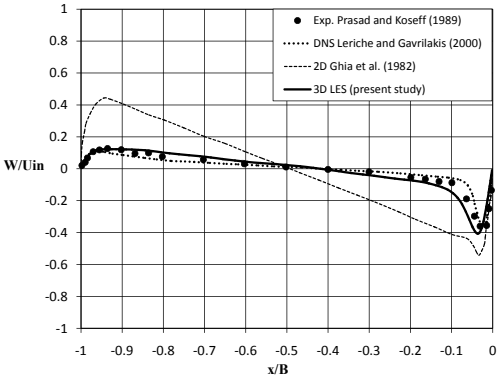

Fig. 12. Comparison of mean w velocities on the centerline ($z/B = 0.5, y/B = 0.5$) in the mid-plane of cavity with experimental data and DNS results. Re=10000 and SAR=1.

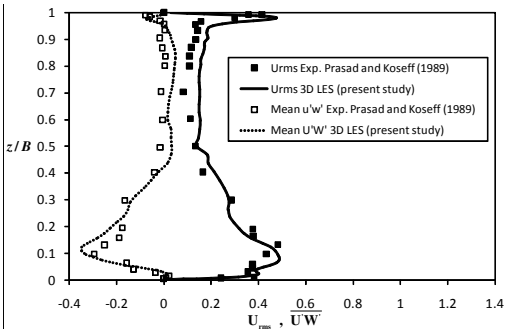

Fig. 13. Comparison of U_{rms} and $\overline{U'W'}$ on the centerline ($y/B = 0.5, x/B = -0.5$) in the mid-plane of cavity with experimental data. Re=10000 and SAR=1.

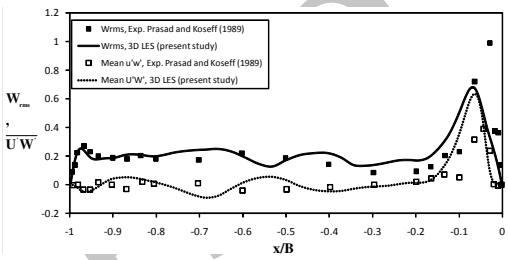

Fig. 14. Comparison of W_{rms} and $\overline{U'W'}$ on the centerline ($z/B = 0.5, y/B = 0.5$) in the mid-plane of cavity with experimental data. Re=10000 and SAR=1.

moves from the bottom to the upstream wall by the spanning act of the primary vortex. The velocity of the flow at upstream wall is reduced.

Based on these figures, t he r esults o f present study show good agreement with experiment Prasad and Koseff (1989) except in mean u velocities near the top lid and in mean w velocities near to the downstream wall, where, some over prediction are observed. The over prediction at this location for u velocity is about 17 % and for w velocity is about 13 %in comparison with experimental data as can be observed in Table 2 . Most of the existent numerical simulations of lid driven cubical cavity with $Re = 10,000$ are based on the $SAR = 0.5$ (Kim and Menon 1999; Huang and Li 2010); where the results of these dynamic LES models show such over-prediction as our results near the downstream wall of cavity.

This over prediction of velocities and thickness of boundary layer may be improved by using finer grids. As can be seen from the Fig. 11 the minimum mean velocity of the flow near the lower wall of cubical cavity equals to $u/U_{in} = -0.22$, where, the agreement with experiment data is good. Also, at upstream wall the numerical results are extremely matched with the experiment. Getting farther from the upstream wall, slight over prediction from the experiment is observed. This over prediction can also be observed in the LES with dynamic SGS of Zang *et al.* (1993) for cubical cavity flow with SAR=0.5 (see Ref. Zang *et al.* (1993). Their results are not presented in the figures). As can be seen in the Fig. 12 , results of the DNS Leriche and Gavrilakis (2000) present very good agreement with experiments with a slight under-prediction for mean down flow velocity near the downstream wall.

In Figs. 13 and 14, root mean square (rms) of velocities in mid plane of the cubical cavity has been depicted and compared to the experimental data of Prasad and Koseff (1989). The quan-

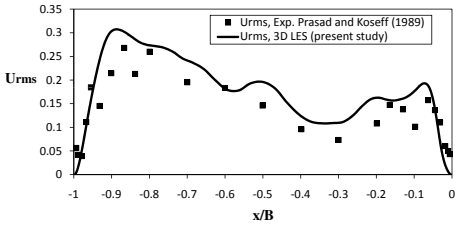

Fig. 15. Comparison of U_{rms} on the centerline ($y/B = 0.5, z/B = 0.5$) in the mid-plane of cavity with experimental data. Re=10000 and SAR=1.

tities of the U_{rms}, W_{rms} and $\overline{U'W'}$ shown in the figures are defined as follows

$$U_{rms} = 10\sqrt{\frac{\widehat{u'^2}}{U_{in}{}^2}}, \quad W_{rms} = 10\sqrt{\frac{\widehat{w'^2}}{U_{in}{}^2}},$$
$$\overline{U'W'} = 350\frac{\widehat{u'w'}}{U_{in}{}^2} \tag{12}$$

where $u' = \bar{u} - \widehat{u}$, $w' = \bar{w} - \widehat{w}$, $u'w' = (\bar{u} - \widehat{u})(\bar{w} - \widehat{w})$ and " $\widehat{.}$ " indicates the time averaging. The values 10 and 350 multiplied in Eq. (12), are due to better presentation of the diagrams.

In Fig. 13 two humps for $\overline{U'W'}$ near the bottom wall are observed in both of the present numerical model and experiment of Prasad and Koseff (1989). In this figure some over prediction in $\overline{U'W'}$ at $z/B = 0.5$ to $z/B \simeq 0.9$ are observed. Note that, the over prediction in mean velocities of u (in Fig. 11) can also be seen in this region. Values of the rms of Reynolds stresses U_{rms} and $U'W'$ are about zero near the upstream wall. It shows that the turbulent stresses are negligible in this region.

In Fig. 14, W_{rms} is in very good agreement with experimental data near the upstream wall of cavity, however, close to the downstream wall the accuracy of the present numerical model is not enough.

In Fig. 15 the values of U_{rms} along the center line of the mid plane of cavity at location $y/B = 0.5, z/B = 0.5$ are shown. The values of U_{rms} have also been calculated using Eq. (12). Qualitative agreement of the U_{rms}s values with the experimental data of Prasad and Koseff (1989) is good except some over-prediction. In this figure the maximum value of error percentage of the numerical results in compari-son with experimental data is about 30%.

4. CONCLUSIONS

In this paper results of a developed numerical model based on the finite volume solution and dual time stepping method on the collocated grids are presented. LES was adopted to deal with the turbulent features of the flow. Turbulent flows in 2-D and 3-D lid driven cavities were chosen to assess the capability and accuracy of the presented numerical code. For 2-D square lid driven cavity, the results presented good agreement with other 2-D numerical results of the researchers. However, discrepancies from the experimental data were observed. This may be due to neglecting of the effects of the side walls in 2-D cavity. For three dimensional cavity flow, good agreements were achieved for both mean and root mean squares of the velocities. Accuracy of the present study with classic LES Smagorinsky model and collocated mesh are acceptable and comparable with other more accurate numerical models like DNS Leriche and Gavrilakis (2000).

ACKNOWLEDGMENTS

The authors gratefully acknowledge the Sheikh Bahaei National High Performance Computing Center (SBNHPCC) for provid-ing computing facilities and time. SBNH-PCC is supported by scientific and techno-logical department of presidential office and Isfahan University of Technology (IUT).

REFERENCES

Aghaee Y. and H. Hakimzadeh (2010, September 8–10). Three Dimensional Numerical Modeling of Flow around Bridge Piers Using LES and RANS. *International conf. of River Flow*, Braunschweig, Germany.

Armfield S. W. (1991). Finite difference solutions of the navier-stokes equations on staggered and non-staggered grids. *comput. Fluids 20* (1), 1–17.

Breuer M. (1993). A dual time-stepping method for 3D, viscous, incompressible vortex flows. *Journal of Comput. Fluids 22* (4), 467–484.

Breuer M. (1998). Numerical and modeling influences on large eddy simulations for the flow past a circular cylinder. *Int. J. Heat and Fluid Flow 19*, 512–521.

Chen D. and G. D. Doolen (1998). Lattice boltzmann method for fluid flows. *Annu. Rev. Fluid Mech 30*, 329–364.

Cheng Y., F. S. Lien, E. Yee and R. Sinclair (2003). A comparison of large Eddy sim-

ulations with a standard k-e Reynolds-averaged Navier-Stokes model for the rediction of a fully developed turbulent flow over a matrix of cubes. *Journal Wind Engineering and industrial Aerodynamics 91*, 1301–1328.

Choi S. (1999). Note on the Use of Momentum Interpolation Method for Unsteady Flows. *Numer. Heat Transfer 36*, 545–550.

Chorin A. J. (1967). A numerical method for solving incompressible viscous flow problems. *Journal of Computational Physics 2*, 12–26.

Cubero A. and N. Fueyo (2007). A Compact Momentum Interpolation Procedure for Unsteady Flows and Relaxation. *Numer. Heat Transfer, part:B 52* (6), 507–529.

Erturk E., T. C. Corke and C. Gokcol (2005). Numerical Solutions of 2-D Steady Incompressible Driven Cavity Flow at High Reynolds Numbers. *J. Numer. Meth. Fluids 48*, 747–774.

Fu W. S., C. G. Li, W. F. Lin and Y. H. Chen (2009). Roe scheme with preconditioning method for large eddy simulation of compressible turbulent channel flow. *Int. J. Numer. Meth. Fluids 61*, 888–910.

Ghia U., K. N. Ghia and C. T. Shin (1982). High-Re Solutions for Incompressible Flow Using the Navier-Stokes Equations and a Multigrid Method. *Computational physics 48*, 387–411.

Gosse L. (2000). A well-balanced flux- vector splitting scheme designed for hyperbolic systems of conservation laws with source terms. *Comput. Math. Appl. 39* (9-10), 135–159.

Hachem E., B. Rivaux, T. Kloczko, H. Digonnet and T. Coupez (2010). Stabilized finite element method for incompressible flows with high Reynolds number. *Journal of Computational Physics 229*, 8643–8665.

Harlow, F. H. and J. E. Welch (1965). Numerical Calculation of Time-Dependent Viscous Incompressible Flow with Free Surface. *Phys. Fluids 8*, 2182–2189.

Harten A. (1983). High resolution schemes for hyperbolic conservation laws. *J. Computat. Phys. 31* (49), 357–393.

Harten A. (1987). High resolution schemes for hyperbolic conservation laws. *J. Computat. Phys. 71*, 231.

Hassan Y. A. and H. R. Barsamian (2001). New-wall modeling for complex flows using the large eddy simulation techniqe in carvilinear coordinates. *J. Heat and Mass Transfer 44*, 4009–4026.

Huang S. and Li Q. S. (2010). A new dynamic one- equation subgrid- scale model for large eddy simulations. *Int. J. Numer. Meth. Engng. 81* (7), 835–875.

Ketabdari M. J. and H. Saghi (2011). Large Eddy Simulation of Laminar and Turbulent Flow on Collocated and Staggered Grids. *International Scholarly Research Network, ISRN Mechanical Engineering 2011*,pp 13.

Khosla P. K. and G. Rubin (1974). A Diagonally Dominant Second Order Accurate Implicit Scheme. *Journal of Comput. Fluids 2*, 207–209.

Kim W. W. and S. Menon (1999). An unsteady incompressible navier-stokes solver for large eddy simulation of turbulent flows. *Int. J. Numer. Meth. Fluids 31*, (6), 983–1017.

Lam K. and Y. F. Lin (2008). Large eddy simulation of flow around wavy cylinders at a subcritical Reynolds number. *Int. J. Heat Fluid Flow 29* (4), 1071–1088.

Marx Y. P. (1994). Time integration schemes for the unsteady incompressible Navier-Stokes equations. *J. Comput. Phys. 112*, 182–209.

Leriche E. and Gavrilakis S., (2000). Direct numerical simulation of the flow in a lid-driven cubical cavity. *Phys. Fluids 12* (6), 1363–1376.

Leriche E. (2006). Direct Numerical Simulation in a Lid- Driven Cubical Cavity at High Reynolds Number by a Chebyshev Spectral Method. *Journal of Scientific Computing 27* (1-3), 335–345.

Li X. S. and C. W. Gu (2010). The momentum interpolation method based on the time- marching algorithm for All-Speed flows. *Computational physics 229* (20), 7806–7818.

Louda P., Kozel K. and J. Prihoda (2008). Numerical solution of 2D and 3D viscous incompressible steady and unsteady flows using artificial compressibility method. *Int. J. Numer. Meth. Fluids* em 56(8), 1399–1407.

Majumdar S., (1988). Role of Under relaxation in Momentum Interpolation for Calculation of Flow with Nonstaggered

Grids. *Numer. Heat Transfer 13*, 125–132.

Miller T. and F. Schmidt (1988). Use of a Pressure-Weighted Interpolation Method for the Solution of the Incompressible Navier-Stokes Equations on a Nonstaggered Grid System. *Numer. Heat Transfer 14*, 213–233.

Muldoon F. and S. Acharya (2007). A modification of the artificial compressibility algorithm with improved convergence characteristics. *J. Numer. Meth. Fluids 55*, 307–345.

Nithiarasu P. (2003). An efficient artificial compressibility (AC) scheme based on the characteristic based split (CBS) method for incompressible flows. *Int. J. Numer. Meth. Engng. 56*, 1815–1845.

Paik J., C. Escauriaza and F. Sotiropoulos (2007). On the bimodal dynamics of the turbulent horseshoe vortex system in a wing-body junction. *Phys. Fluids. 19*, 045107-1–20.

Prasad A. k. and J. R. Koseff (1989). Reynolds number and end-wall effects on a lid-driven cavity flow. *Phys. Fluids A*, *1*, 208–218.

Premnath K., M. J. Pattison and S. Banerjee (2009). Generalized Lattice-Boltzmann Equation with Forcing Term for Computation of Wall-Bounded Turbulent Flows. *Phys. Rev. E 79* (2),0–19.

Prokop V. and Kozel K. (2010). Numerical simulation of Newtonian and non-Newtonian flows in bypass. *Mathematics and Computers in Simulation 80*, 1725–1733

Rhie C. and Chow W. (1983). Numerical Study of the Turbulent Flow Past an Airfoil with Trailing Edge Separation. *AIAA J. 21* (11), 1525–1532.

Roy A. and Bandyopadhyay G., (2006). A finite volume method for viscous incompressible flows using a consistent flux reconstruction scheme. *J. Numer. Meth. Fluids 52*, 297–319.

Sahin M. and R. G. Owens (2003). A novel fully implicit finite volume method applied to the lid-driven cavity problem-Part I: High Reynolds number flow calculations. *J. Numer. Meth. Fluids 42*, 57–77.

Shankar P. N. and M. D. Deshpande (2000). Fluid mechanics in the driven cavity. *Annu. Rev. Fluid Mech. 32*, 93–136.

Sheu T. W. H. and R. K. Lin (2004). Newton linearization of the incompressible Navier-Stokes equations. *Int. J. Numer. Meth. Fluids 44*, 297–312.

Steger J. L. and Warming R. F. (1981). Flux vector splitting of the inviscid gas dynamic equations with application to finite difference methods. *J. Computat. Phys. 31*, 40, 263–293.

Strikwerda J. C. (1984). Finite difference methods for the Stokes and Navier-Stokes equations. *SIAM J. Sci. Statist. Comput. 5*, 65–68.

Tamamidis Y., G. Zhang and D. N. Assanis (1996). Comparison of Pressure-Based and Artificial Compressibility Methods for Solving 3D Steady Incompressible Viscous Flows. *Journal of Computational Physics 124*, 1–13.

Yu B., W. Kawaguchi, Q. Tao and H. Ozoe (2002). Checkerboard Pressure Predictions due to the Underrelaxation Factor and Time Step Size for a Nonstaggered Grid with Momentum Interpolation Method. *Numer. Heat Transfer 41*, 85–94.

Zang Y. R., L. Street and J. R. Koseff (1993). A dynamic mixed subgridscale model and its application to turbulent recirculating flows. *Phys. Fluids A 5*, 3186–3196.